UNIVERSITAT POLITÈCNICA DE CATALUNYA BARCELONATECH

UPCommons

Portal del coneixement obert de la UPC

http://upcommons.upc.edu/e-prints

Aquesta és una còpia de la versió *author's final draft* d'un article publicat a la revista *Microchimica acta*.

URL d'aquest document a UPCommons E-prints:
http://hdl.handle.net/2117/165258

Article publicat / *Published paper*:

Amperometric thyroxine sensor using a nanocomposite based on graphene modified with gold nanoparticles carrying a thiolated β-cyclodextrin

Jose Muñoz[1] · Marta Riba-Moliner[2] · Lorcan J. Brennan[3] · Yurii K. Gun'ko[3,4] ·
Francisco Céspedes[1] · Arántzazu González-Campo[2] · Mireia Baeza[1]

Abstract This article reports a novel electrochemical sensor based on a nanocomposite for the sensitive determination of Thyroxine (T_4), the active form of the hormone. Hydrodynamic amperometry is performed with a nanocomposite electrode based on the dispersion of a graphene–based filler hybrid-nanomaterial throughout an insulating epoxy resin in the optimum composition ratio (the near–percolation composition). This hybrid-nanomaterial consists of reduced graphene oxide tuned with gold nanoparticles and a biorecognition agent, the thiolated β-cyclodextrin. Recognition of T_4 is accomplished via supramolecular chemistry, due to the formation of an inclusion complex between β-cyclodextrin and T_4. The amperometric device operates at +0.85 V vs. Ag/AgCl, where the oxidation of T_4 takes place on the electrode surface. The sensor covers the 1.00 nM to 14 nM T_4 concentration range in a 0.1 M HCl solution, with a detection limit of 1.00 ± 0.02 nM. The sensor can be easily reset by polishing. It exhibits the lowest detection limit regarding to any other electrochemical electrodes for T_4 determination previously described in literature.

Introduction

Thyroxine (T_4) is an important biological hormone which can be considered as an iodoamino acid derivative of thyronine, produced in the thyroid gland. The determination of T_4 has practical clinical significance for the diagnosis of hyperthyroidism and hypothyroidism [1, 2]. For this reason, a wide range of analytical methods for the detection of T_4, including immunoassay [3], chemiluminescence [4], mass spectroscopy [5] and high performance liquid chromatography [6], among others, have been developed. However, these methods are complicated and require expensive instruments. Electrochemical techniques open new alternatives to develop facile and easy to automate analytical methodologies. The electrochemical response of T_4 has previously been investigated using silver and mercury electrodes [7, 8]. Some carbon–based electrodes have also been studied, such as chemically modified carbon paste electrodes (with or without the presence of surfactants) [9, 10] or carbon nanotubes modified glassy carbon electrodes [11]. In spite of that, graphene–based electrodes have not been directly used for T_4 detection.

Comparing to conventional solid carbon electrodes, as the typical glassy carbon electrodes or other metal electrodes, graphene–based nanocomposite electrodes present a series of benefits, such as robustness from the host polymer to the final composite electrode and an easy surface renewal, as well as a randomly exposed filler material on the electrode surface.

✉ Arántzazu González-Campo
agonzalez@icmab.es

✉ Mireia Baeza
mariadelmar.baeza@uab.cat

1   Departament de Química, Facultat de Ciències, Edifici C-Nord, Universitat Autònoma de Barcelona, 08193 Cerdanyola del Vallès, Bellaterra, Spain

2   Functional Nanomaterials and Surfaces Group, Institut de Ciencia de Materials de Barcelona (ICMAB-CSIC), Campus de la UAB, 08193 Cerdanyola del Vallès, Bellaterra, Spain

3   School of Chemistry and CRANN Institute, Trinity College Dublin, Dublin 2, Ireland

4   International Research and Education Center for Physics of Nanostructures, ITMO University, 197101 Saint Petersburg, Russia

These types of devices can be easily integrated as a detector in an automated flow injection analysis system, with the additional benefits of providing a highly sensitive analyzer for the rapid determination of T_4 [12]. Otherwise, depending on the conductive load and its distribution through the insulating polymeric matrix, nanocomposites can behave as microelectrode arrays [13]. From an electrical point of view, working with near-percolation composite (NPC) (bio)sensors guarantees an improvement of electroanalytical properties, such as higher signal-to-noise ratios and lower detection limits for a variety of reagents [14]. Under this context, the optimization of the conductive phase loading is a key point for improving their final electroanalytical performance.

The potential scope of graphene–based nanocomposite sensors is enormous. Graphene based materials present improvements in their electrochemical properties comparing to conventional carbon materials [15] such as graphite or carbon nanotubes, mainly attributed to the presence of more sp^2-like planes and edge defects in graphene [16, 17]. As another important member of graphene family, Graphene Oxide (GO) and reduced Graphene Oxide (rGO) are more electrochemically active as compared to pristine graphene. Nevertheless, the main limitation of GO is the disruption of the sp^2 carbon network which dramatically reduces electronic transport across the 2D sheet. The reduction of GO partially restores the conductivity, resulting in a nanomaterial with reasonably good conductivity, as well as thermal stability and processability [18, 19]. For instance, nanostructuring provides an enhancement of the biocompatibility and a facile tunability with different types of nanoparticles, including Au–NPs. In recent years, many studies of carbon–based metal nanocomposites have been reported, because of their interesting electrical, optical and magnetic properties [20]. Nanohybrids films materials based on reduced graphene containing Au–NPs (Au–NP@rGO) provides an optimal microenvironment for (bio)molecule immobilization and facilitate electron transfer between the (bio)molecule and conducting hybrid-nanomaterial, which have been widely applied in biosensors for the detection of proteins, bacteria and cells [21, 22]. The use of biorecognition agents can preconcentrate the analyte on the electrode surface, resulting in more sensitive sensors, achieving lower detection limits.

β–cyclodextrin (β–CD) is a (bio)recognition agent that can host effectively, selectively and enantioselectivily various organic, inorganic and biological guest (bio)molecules into their hydrophobic cavities [23, 24] forming a stable host-guest inclusion complex or nanostructure supramolecular assemblies, including T_4 [25]. However, it is rarely reported work regarding the synthesis of gold nanoparticles–graphene nanohybrid and the application in biorecognition systems.

In this sense, a system based on Au–NP@rGO with attached thiolated-β–CD (β–CD-SH) seems to be a suitable and alternative conducting hybrid-nanomaterial

filler which can readily be dispersed in an insulating polymeric matrix (the epoxy resin) for the development of rigid amperometric nanocomposite sensors for the sensitive determination of T_4, as is depicted in Scheme 1.

## Materials and methods

Chemicals and reagents

GO was synthesized from flaked graphite (Alfa Aesar, Karlsruhe, Germany). Reduced Graphene Oxide (rGO) was obtained through the reduction of GO using ascorbic acid. Epotek H77A and its corresponding hardener Epotek H77B, from Epoxy Technology (Billerica, MA, USA), were used as the polymeric matrix. All solutions were prepared using deionized water 18.2 MΩ·cm from a Milli-Q system (Millipore, Billerica, MA, USA). Potassium ferricyanide/ferrocyanide (99.8 %), ascorbic acid (99.5 %), sodium nitrate (99.0 %), potassium chloride (99.5 %), nitric acid (65 %), potassium permanganate (99.99 %), sulphuric acid (95–98 %), hydrochloric acid (30–35 %), hydrogen peroxide (30 %) and gold dichloride hydrochloride (> 99.99 %) were purchased from Sigma-Aldrich (St. Louis, MO, USA). Levo-Thyroxine (T_4, 3,5,3′,5′-tetraiodothyroxin, >98 %) has been was also procured from Sigma-Aldrich and used without further purification. Stock solution of 5 mM T_4 was prepared by dissolving it in a 0.1 M ethanolic NaOH solution, which was stored in dark at 4 °C. Standard solutions were prepared by the dilution of the stock solution. Thiolated β-cyclodextrin (per-6-thio-β-cyclodextrin, β-CD-SH) was synthesized following the established methodology [26].

Synthesis of hybrid-nanomaterials related to graphene

GO was synthesized from natural graphite powder via Hummers method [27]. The product was washed several times through centrifugation with a 10 % aqueous solution of hydrochloric acid followed by copious amounts of water until the pH was ~6. Finally, the product was dried overnight at 80 °C.

Synthesis of hybrid-nanomaterials was carried out by an environmentally friendly technique. For the synthesis of rGO containing gold nanoparticles (Au–NP@rGO), 350 mg of GO was dispersed in 250 mL of Milli-Q water and ultrasonicated for 1 h. After ultra-sonication, the aqueous GO suspension was added to a 500 mL round bottomed flask and set to stir at room temperature for 30 min. Then, $2.5 \cdot 10^{-3}$ mol of HAuCl$_4$ (precursor for Au–NPs synthesis) was added to the suspension and left to stir for another 30 min. The solution was reduced with 250 mL of an aqueous 0.1 M NaBH$_4$ solution, which was added drop wise to the reaction vessel. The solution was left to stir for a further 1 h. Following this, the functionalized nanomaterial (Au–NP@rGO) was washed

Scheme 1 Synthetic route of Au–NP@rGO and β–CD-SH/Au–NP@rGO hybrid-materials from GO and their subsequently dispersion in epoxy resin for nanocomposite sensor purposes
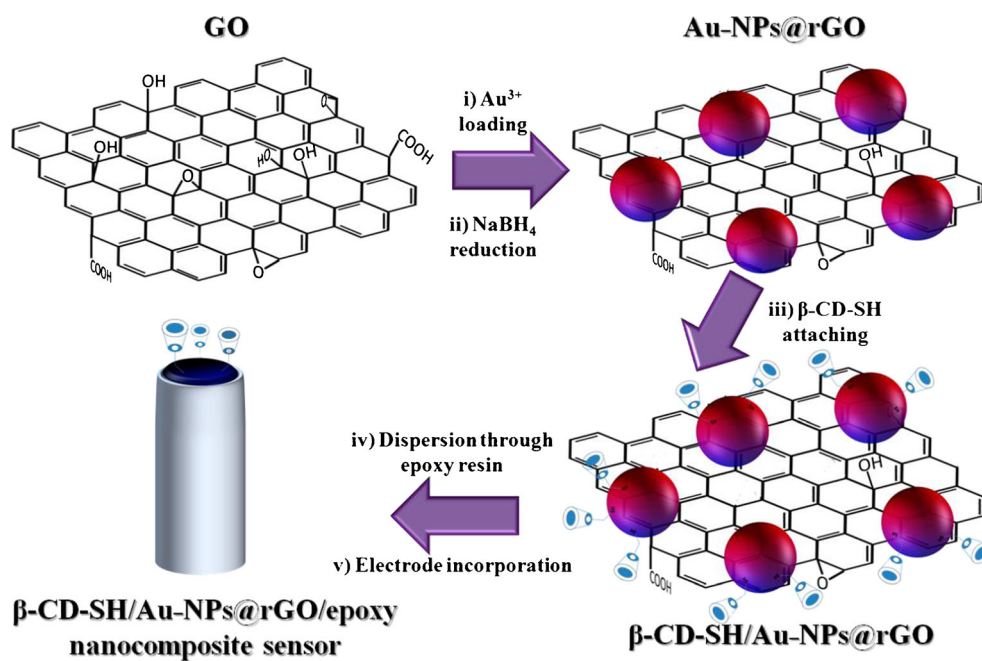
several times with water through a high speed centrifugation for 10 min. Once the Au–NP@rGO hybrid-nanomaterial was obtained, the resultant product was dispersed in 250 mL of Milli-Q water and ultra-sonicated for 1 h. Then, the aqueous Au–NP@rGO suspension was added to a 500 mL round bottomed flask and set to stir at room temperature for 30 min. Following this, 250 mL of an aqueous (9:1 water/ethanol, *v*/v) 2.0 mM suspension of β–CD-SH was added. The solution was left to stir overnight. Afterwards, the product was centrifuged for 10 min and washed several times with Milli-Q water and ethanol, in order to remove the unbound β–CD-SH. The resultant product (β–CD-SH/Au–NP@rGO) was dried overnight at 80 °C.

Percolation experiments were carried out using rGO/epoxy nanocomposite electrodes from 8 % to 20 % in rGO loading (*w*/w). The rGO was used as the conducting nanofiller material. In this case, rGO was obtained through the reduction of GO using ascorbic acid as a reducing agent [28].

Characterization of hybrid-nanomaterials

Physical characterization of the different carbon nanomaterials was carried out using different techniques. Images of GO, Au–NP@rGO and β–CD-SH/Au–NP@rGO were obtained from High-Resolution Transmission Electron Microscopy (HR–TEM), using a JEM-1400 unit with an acceleration voltage of 120 kV coupled to an Energy Dispersive X-Ray Spectroscopy (EDS). Approximately 0.1 mg of sample was dispersed in 10 mL of Milli-Q water as solvent and then placed in ultrasound bath for 2 h. Finally, a drop of this solution was placed on a gold grid and let it dry before HR-TEM and EDS analysis.

Thermogravimetric Analysis (TGA) technique was used to quantify the total metal content in the hybrid materials. The experiments were carried out using a Netzsch instrument; model STA 449 F1 Jupiter®. Approximately 20 mg of sample was heated to 1000 °C at 10 °C/min, using air flow. The mass of the sample was continuously measured as a function of temperature and the rate of weight loss (d.t.g.) was automatically recorded. The number of the β–CD-SH per Au–NPs has been measured following the supporting information from Tom's work [29].

The optical characteristics of the graphene–based materials were monitored using UV-vis spectroscopy (Agilent Technologies, Cary 60 Uv-Vis scanning spectrometer).

Preparation of nanocomposite electrodes

Handmade working nanocomposite electrodes were prepared by mixing the polymer Epotek H77A and its corresponding H77B hardener in a 20:3 (*w*/w) ratio and adding different amounts of rGO as conducting filler nanomaterial for percolation studies of rGO/epoxy nanocomposite sensors (from 8 % to 20 % *w*/w in rGO loading). For the preparation of nanocomposite electrodes based on hybrid-nanomaterials (Au–NP@rGO/epoxy and β–CD-SH/Au–NP@rGO/epoxy nanocomposite electrodes), only an optimum loading of conducting nanofiller (13 % *w*/w in Au–NP@rGO or β–CD-SH/Au–NP@rGO) was used. Both types of conducting fillers were dispersed in the epoxy resin and hardener agents through manually homogenization for 30 min. For the electrode construction, the nanocomposite was placed into a cylindrical polyvinyl chloride (PVC) tube (6 mm of internal diameter and 20 mm of length) containing a

copper disk (5 mm of diameter and 1 mm of thickness) soldered to an electrical connector end (2 mm of diameter), as is depicted in Fig. 1. Prior to soldering, the copper disk was treated with a 5 % HNO_3 solution v/v for 2 min in order to remove the oxide layer. The mixture was then incorporated in the hollow end of a PVC tube to form the body of the electrode. The final paste-filled cavity was 3 mm long inside the PVC tube. Then, the nanocomposite paste electrodes were allowed to harden during 24 h at 80 °C [30]. Afterwards, in order to obtain a reproducible electrochemical surface, electrode surfaces were polished with different sandpapers of decreasing grain size (800 and 1200) and finally with alumina paper (polishing strips 948,201, Orion). The resultant geometric area for the final electrodes was 28 mm^2.

Finally, for the β–CD-SH/rGO/epoxy nanocomposite electrode preparation, filler nanomaterial (rGO) and recognition agent (β–CD-SH) were dispersed through the polymeric matrix according to the ratio obtained by TGA analysis (see *Section 3.1*) for β–CD-SH/Au–NP@rGO (11.4 % in rGO and 1.6 % in β–CD-SH, w/w).

Characterization of nanocomposite electrodes

The percolation curve of the rGO/epoxy nanocomposite electrodes was carried out through measurement of the electrical resistance, which were performed using a digital multimeter (Fluke, Everett, WA, USA). The electrical resistance was measured between the copper piece of the connector and the nanocomposite electrode surface. Three equal nanocomposite electrodes were fabricated and evaluated for each composition (from 8 % to 20 % in conducting filler nanomaterial, w/w) in order to estimate the reproducibility of the hand-made fabrication. Five different points were tested for each nanocomposite electrode to study the repeatability of the measurements.

Electrochemical experiments were carried out by Cyclic Voltammetry (CV), using a pontentiostat/galvanostat Autolab system (PGSTAT 30 and FRA boards, Eco Chemie, Utrech, The Netherlands) with a three-electrode configuration. The system was run on a PC using GPES and FRA 4.9 software. A single junction reference electrode Ag/AgCl Orion 900,200 (Thermo Electron Corporation, Beverly, MA, USA) and a platinum–based electrode 52–671 (Crison Instruments, Alella, Barcelona, Spain) were used as reference and auxiliary electrodes, respectively. The nanocomposites were employed as working electrodes. The measurements were made in 10.0 mL of 0.1 M HCl supporting electrolyte for T_4 detection at different scan rates (from 5 to 100 $mV·s^{-1}$) in order to achieve the optimum scan rate, which was found at 50 $mV·s^{-1}$. An additional electrochemical characterization was also carried out in a 0.1 M KCl solution containing 0.01 M $[Fe(CN)_6]^{3-/4-}$ to study the electrochemical behavior of the different graphene–based nanocomposite electrodes. All the experiments were performed at room temperature (25 °C).

Electroanalytical experiments were made using an amperimeter LC-4C (Bioanalytical Systems, Inc., West Lafayette, IN, USA) in a 10.0 mL 0.1 M HCl solution with a three-electrode configuration [31]. Amperometric measurements were performed under stirring conditions at 850 mV vs. Ag/AgCl fixed potential. Detection limit (LOD) and quantification limit (LOQ) were calculated three times ($n = 3$) and they are presented with their respectively 95 % confidence interval [32]. To estimate the reproducibility of the nanocomposite materials, three different sensors were evaluated for each nanocomposite.

Results and discussion

Motivated by the possibility of developing an alternative rigid carbon composite sensor for the sensitive, fast and inexpensive determination of T_4, graphene has been chosen as a novel conducting nanofiller material for nanocomposite electrodes fabrication. In comparison with carbon nanotubes, graphene present significant advantages such as it does not contain metallic impurities and is produced from flacked graphite, which is economical and accessible. Due to the non-conducting nature of GO, the reduction of GO (rGO) partially restores the conductivity, resulting in a nanomaterial with reasonably good conductivity. In order to improve the sensitivity of the electrode for the detection of T_4, β–CD-SH was used as biorecognition element in a nanocomposite sensor. For the successful attachment of the thiolated-biorecognition agent
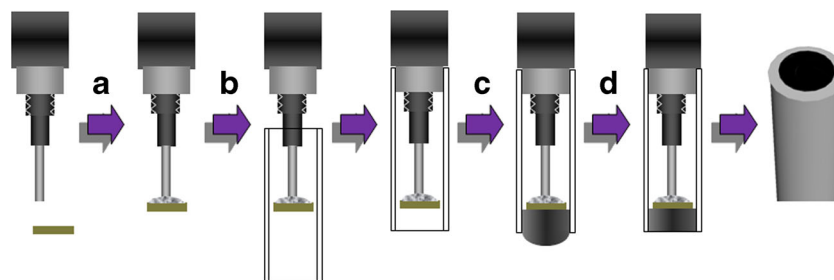

Fig. 1 Stages for the construction of an electrode. **a** A copper disk is soldered to a 2 mm female connector. **b** Afterwards, it is introduced into a PVC tube. **c** The filler/epoxy nanocomposite paste is incorporated in the hollow end of a PVC tube to form the body of the electrode. **d** Finally, the nanocomposite paste is cured and polished, obtaining the working electrode

to the conducting nanofiller material, Au–NPs were previously incorporated on the graphene layers as nanotemplates. The presence of Au–NPs is essential in order to maintain the conductivity of the nanocomposite. The strength of the gold-thiol interactions provided the basis for obtaining a robust hybrid-nanomaterial [33].

Physical characterization of hybrid-nanomaterials

HR–TEM images were taken for the different graphene–based nanomaterials. Figure 2 a verified the successful synthesis of GO from the bulk graphite. HR–TEM micrograph in Fig. 2b depicts a representative image of the deposition of Au–NPs upon the graphene sheets, resulting the Au–NPs@rGO hybrid nanomaterial. Analysis of the images from Fig. 2b and c show clearly a homogeneous distribution of Au–NPs on the graphene surface with an average particle size of 5.6 ± 0.9 nm. EDS spectrum of Au–NP@rGO qualitatively determined the presence of Au–NPs on the graphene sheets (see Fig. 2d). Figure 2e depicts the resulting β–CD-SH/Au–NP@rGO hybrid-nanomaterial after attaching β–CD-SH. Its corresponding EDS spectrum (Fig. 2f) confirmed the presence of the sulphur peak provided by the incorporation of β–CD-SH.

UV-vis spectra recorded for GO and Au–NP@rGO can be seen in Fig. 3. The main spectroscopic features associated with optical absorption in GO (a) are the electronic transitions

Fig. 2 HR–TEM images of **a** GO; **b** Au–NP@rGO; **c** Au–NP@rGO magnification and **d** its corresponding EDS. **e** HR–TEM image of β–CD-SH/Au–NP@rGO and **f** its corresponding EDS spectra
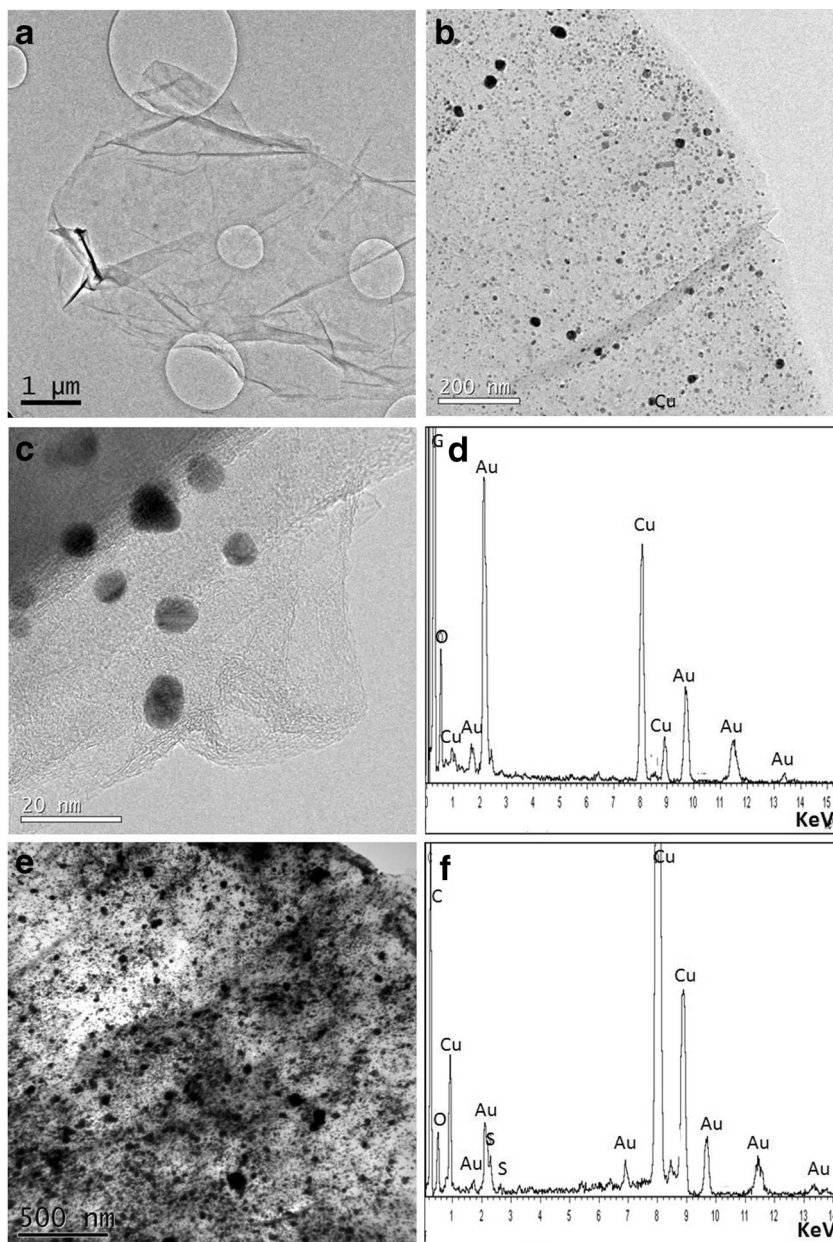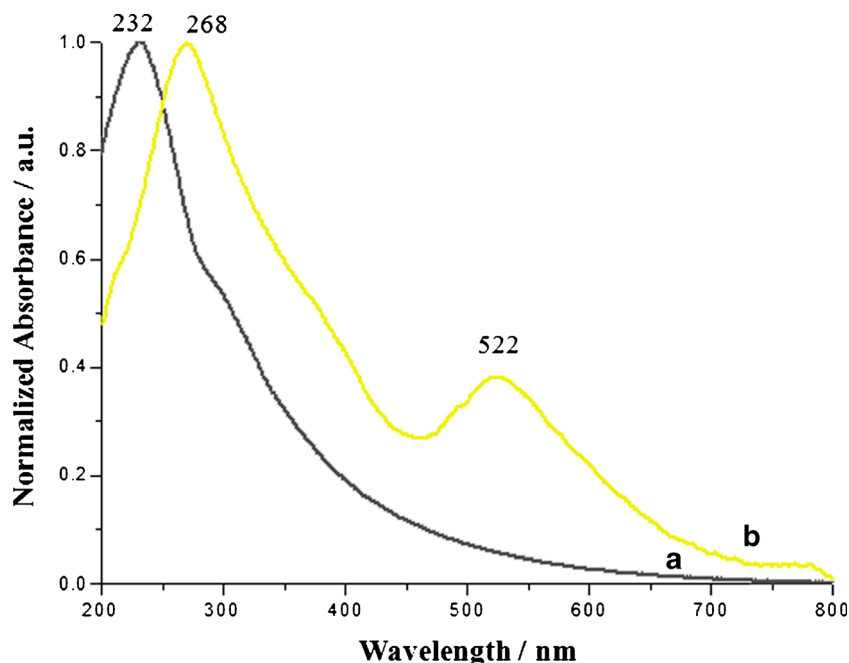
Fig. 3 UV–vis spectra recorded for aqueous suspension of **a** rGO and **b** Au–NP@rGO

within –C = C bonds (232 nm) and –C = O bonds (~300 nm). After reduction has taken place under Au^{3+} loading with $NaBH_4$ for Au–NP@rGO formation (b), the band associated with –C = O functionality is removed from the spectra while the band located at 232 nm shifts to the red (268 nm) due to an increase in the in-plane sp^2 hybridization [34]. Au nanospheres typically show a band around 520 nm in the visible spectrum due to the surface plasmon resonance [35]. Accordingly, the second band located at 522 nm observed in the Au–NP@rGO hybrid-nanomaterial is associated with the presence resonance of Au–NPs on the rGO surface, indicating the successful mobilization of Au–NPs on the nanostructured carbon material.

A quantitative determination of the wt% of Au–NPs and β–CD-SH on the graphene sheets was determined by TGA, which determined an amount of 23.6 wt% of Au–NPs and 12.5 wt% of β–CD-SH. This is an excellent result which shows the importance of Au–NPs incorporation on the rGO sheet. The presence of such a high wt% of Au-NPs facilitates the binding of a large content of β–CD-SH molecules. The resulting number of β-cyclodextrins per Au–NPs (with an average diameter of 5.6 nm) is $n_{β–CD-SH} \approx 230$.

Electrical characterization

Different rGO/epoxy loadings (from 8 % to 20 % *w*/w in nanofiller material) were previously investigated following the percolation theory [36, 37] as it is shown in Fig. 4. The percolation curve displayed the optimum nanocomposite composition interval (the near–percolation zone, NPC zone), which was found to be between 12 % and 14 % (*w*/w) in

nanofiller material loading. In this zone, the resistivity of the nanocomposite material decreases to the current flow. Working with NPC electrodes ensures an effective electron transfer as well as high signal-to-noise ratio [14, 38]. The benefits of using this approach are better detection limits, wider lineal range and increase of the stability as well as the repeatability of the analytical signal. Moreover, the reproducibility in the electrode production is slightly affected using the NPC electrodes. Accordingly, 13 % *w*/w of conducting nanofiller hybrid-material was chosen as the optimal
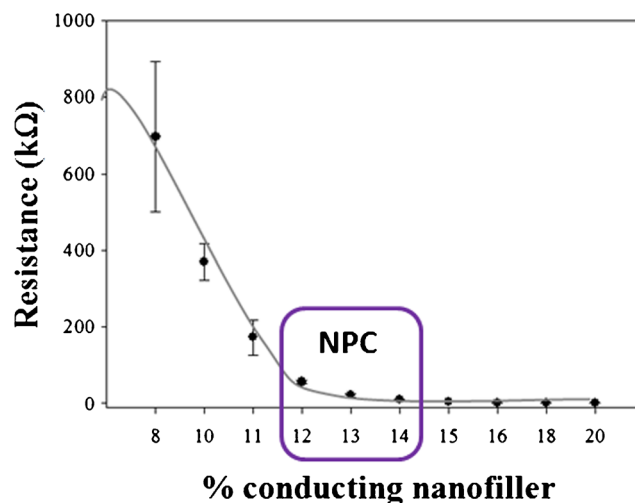

Fig. 4 Percolation curve of rGO/epoxy nanocomposite electrodes, from 8 % to 20 % (*w*/w) in rGO loading. The NPC zone is found between 12 % and 14 % in rGO loading. Experiments were made five times with three different nanocomposite electrodes (*n* = 15) and are presented with their respectively 95 % confidence interval

composition ratio for the electrode construction and therefore, for electroanalytical experiments.

Electrochemical performance of the nanocomposite electrodes

Having optimized the optimum composition ratio, the electrochemical behavior of the different nanocomposite electrodes (rGO/epoxy, Au–NP@rGO/epoxy, β–CD-SH/Au–NP@rGO/epoxy and β–CD-SH/rGO/epoxy) were studied via CV (see Fig. 5). Comparing to the bare rGO/epoxy nanocomposite electrode, an increase of the peak height was observed when Au–NPs were incorporated on the graphene sheets. This enhancement can be attributed to the electrocatalytic effect of the functional metal nanoparticles on electrochemical systems [39]. However, when the β–CD-SH was attached upon these nanoparticles, current height value significantly decreased mainly caused by the steric hindrance of these molecules on the electrode surface, as well as its insulating behavior. In spite of that, the β–CD-SH/Au–NP@rGO/epoxy nanocomposite electrode still maintains an excellent electrochemical performance. In order to demonstrate the importance of the Au–NPs as a supporting nanotemplate, a fourth nanocomposite material, the β–CD-SH/rGO/epoxy electrode, was also electrochemically evaluated. Figure 5 also shows how the introduction of the equivalent amount of β–CD-SH obtained by TGA in powder form directly into the epoxy rGO/epoxy nanocomposite resulted in a strong loss of conductivity. These results may be explained since the β–CD-SH can directly interact with the conducting rGO filler and block the electron transfer. Similar behavior has been observed for GO, which is a non-conducting material. Under this context, the
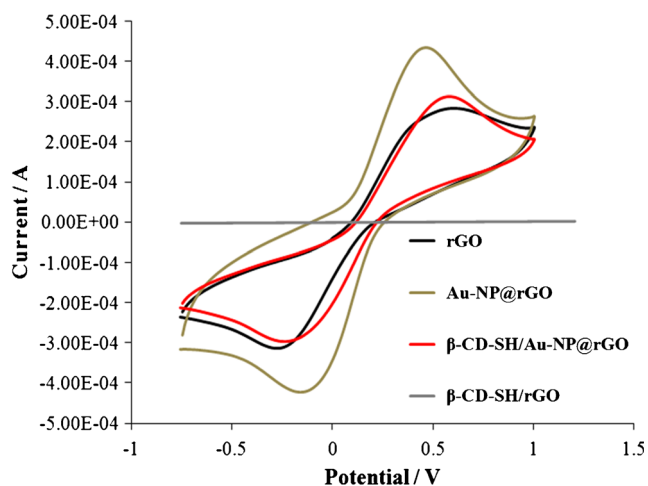
introduction of the Au–NPs is of vital importance in maintaining the conductivity of the nanocomposite device.

Three different conducting graphene–epoxy nanocomposite electrodes (rGO/epoxy, Au–NP@rGO/epoxy and β–CD-SH/Au–NP@rGO/epoxy) were electrochemically characterized by CV under the presence of 10 μM T_4 in a 0.1 M HCl solution, as is shown in Fig. 6. Electrodes containing Au–NPs (Au–NP@rGO/epoxy and β–CD-SH/Au–NP@rGO/epoxy nanocomposite electrodes) present a pair of well-defined anodic and cathodic peaks (E_{a1}/E_{c1}), attributed to the oxidation and the consequent reduction of the Au–NPs. However, the bare rGO/epoxy nanocomposite electrode does not show this pair of peaks, as was expected. Otherwise, whereas the introduction of the biorecognition agent on the device considerable increases the current signal of the T_4 oxidation (E_{a2}) at the β–CD-SH/Au–NP@rGO/epoxy electrode, the response of T_4 on the bare rGO/epoxy and Au–NP@rGO/epoxy electrode surfaces appeared weak and broad. This increase on the oxidation peak current verifies an excellent supramolecular interaction between β-cyclodextrin and the T_4. In comparison to the electrodes without the β-cyclodextrin-SH, the current signal improved 40 %.

Voltammetric studies

The electrochemical response of 10 μM T_4 in a 0.1 M HCl solution [31] at the β–CD-SH/Au–NP@rGO/epoxy nanocomposite electrode was also characterized by CV. Figure 7a depicts the influence of scan rate (5–100 mV·s^{-1}) on the electrochemical response of T_4. The peak current is dependent upon the T_4 oxidation on the electrochemical surface. A pair of well-defined anodic and cathodic peaks (E_{a1}/E_{c1}) is also
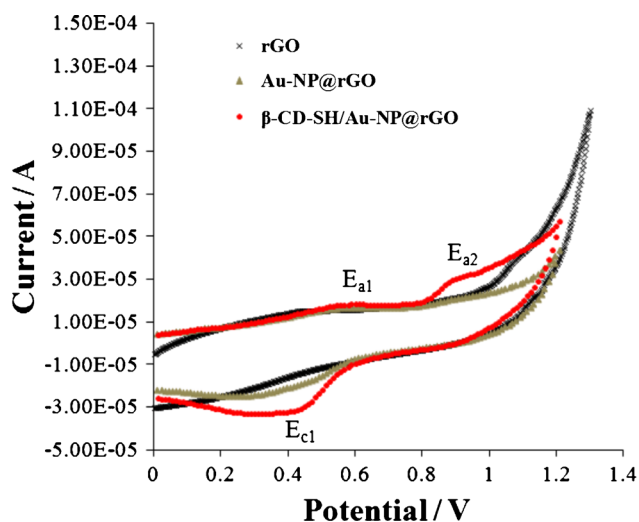

Fig. 5 Electrochemical behavior of the different graphene–based nanocomposite electrodes in a 0.1 M KCl containing 0.01 M [Fe(CN)$_6$]$^{3-/4-}$. Experiments were carried out by cyclic voltammetry (scan rate: 50 mV·s^{-1})

Fig. 6 Cyclic voltammograms of the different graphene–epoxy nanocomposite electrodes under the presence of 10 μM of T_4 in a 0.1 M HCl solution. Scan rate: 50 mV·s^{-1}

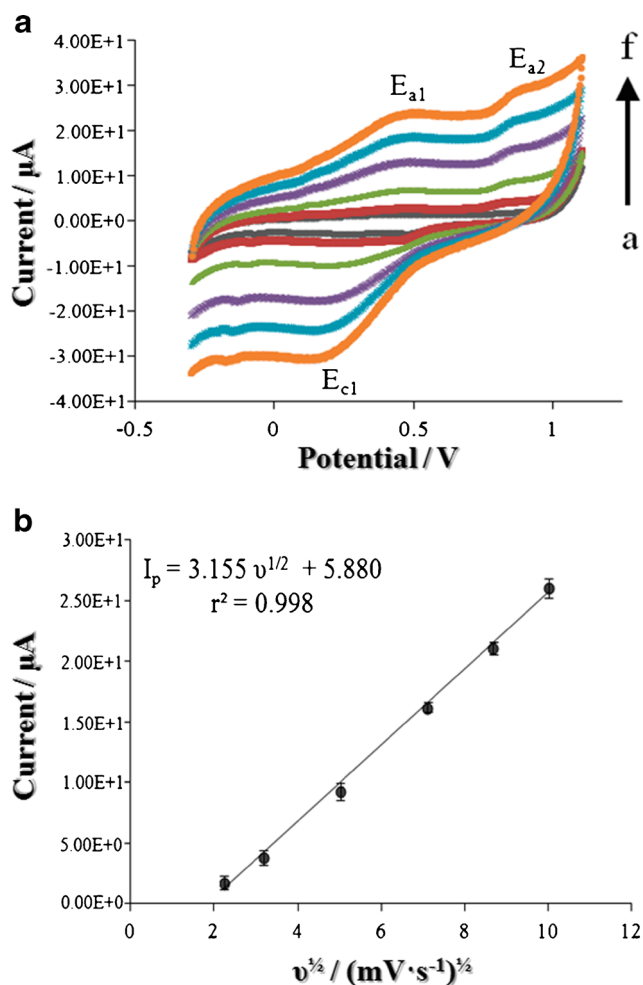**Fig. 7** **a** Influence of scan rate from a 5 to f) 100 mV·s^{-1} for T$_4$ sensing at the β–CD-SH/Au–NP@rGO/epoxy nanocomposite electrode. **b** Anodic peak currents vs. square root of the scan rates (*n* = 9). Voltammetric experiments were carried out in a 0.1 M HCl solution under the presence of 10 μM of T$_4$

possible to be observed from Fig. 7a, which are believed to be due to the redox reaction of Au–NPs. This pair of peaks (E$_{a1}$/E$_{c1}$) was found around +0.55 V vs. Ag/AgCl (E$_{a1}$) and +0.40 V vs. Ag/AgCl (E$_{c1}$), corresponding to the formation and subsequent reduction of gold oxide, respectively [40]. Moreover, the electrochemical behavior of T$_4$ is shown in Fig. 7a. A well-defined oxidation peak (E$_{a2}$) appeared at around +0.85 V vs. Ag/AgCl for the β–CD-SH/Au–NP@rGO/epoxy electrode, which is in concordance with the previously reported carbon–based electrodes in this acidic medium [41].

Figure 7b depicts how the anodic peak currents varied linearly with the square root of the scan rates. This fact indicates a diffusion-controlled process of the oxidation of T$_4$. The optimal scan rate was selected at 50 mV·s^{-1}, which ensures a suitable current for T$_4$ detection. Multiple CVs confirmed the irreversible oxidation of T$_4$, which also occur in nature, since

no reverse peaks were observed (data not shown). After the successive voltammetric cycles at fixed scan rate of 50 mV·s^{-1} the anodic current response for T$_4$ gradually decreased. This fact indicates that the oxidized product blocked the electrode surface and consequently, the possibility to determine more T$_4$ present in the solution

Electroanalytical performance at the sensor

It is worthy to note that the CV method for the determination of T$_4$ presented the limitation of surface fouling by adsorption during the pre-concentration process. In order to develop more accurate methods for detection of T$_4$, hydrodynamic amperometric experiments were carried out, enabling a more sensitive technique rather than the CV methodology. Amperometric calibration curve was performed for the β–CD-SH/Au–NPs@rGO/epoxy sensor in a 0.1 M HCl solution with subsequent additions of 1.0 μM T$_4$ aliquots (see Fig. 8). The polarization potential applied was +0.85 V vs. Ag/AgCl.

As is depicted in Fig. 8, the calibration curve obtained was, I$_p$ (nA) = 2.485 ± 0.005 [T$_4$] (nM) − 2.458 ± 0.008, with r^2 = 0.999 (*n* = 9), together with a detection limit (LOD) of 1.00 ± 0.02 nM and a quantification limit (LOQ) of 2.00 ± 0.03 nM. The LOD of the novel nanocomposite sensor containing β–CD-SH was obviously improved regarding to those previously referenced electrodes using another carbon materials (modified or not) as working electrodes, which are summarized in Table 1. This analytical enhancement may be attributed to a combination of two factors: the 2D nanofiller material and the biorecognition agent, promoting electron transfer in the oxidation of T$_4$ on the electrode surface.
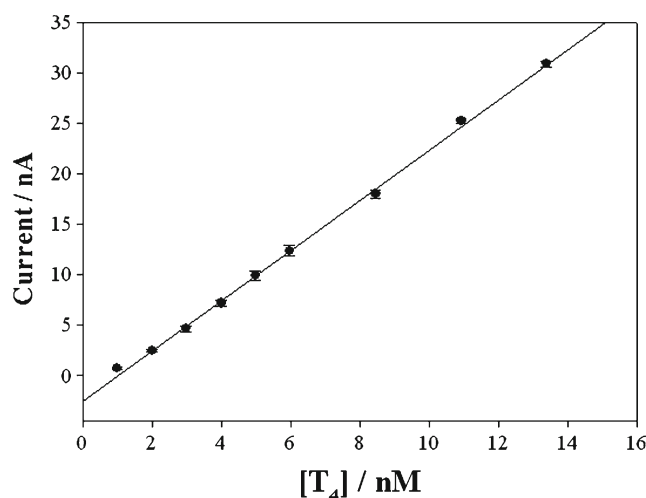

Fig. 8 Calibration curve of [T$_4$] vs. current carried out by hydrodynamic amperometry in a 0.1 M HCl solution; E$_{app}$: +0.85 V vs. Ag/AgCl. LOD and LOQ were calculated three times (*n* = 3) and they are presented with their respectively 95 % confidence interval

Table 1 Comparison of sensing performance for T_4 oxidation and its determination with different carbon–based electrochemical electrodes

Electrodes	Electrochemical tool	Redox potential (V)	LOD* (nM)	References
Phenylhydrazine mediated CPE[1]	CV	0.78	2500	[31]
Polyvinylpyrrolidone modified CPE (in CMAB[2] media)	CV	0.42	80	[10]
Carbon Nanotube film on a GCE[3]	DPV	0.80	6.5	[11]
Edge-Plane PGH[4]	CV	0.82	3.0	[43]
Unmodified SPCE[5]	DPV	0.30	3.0	[44]
β–CD-SH/Au–NP@rGO/epoxy	Amperometry	0.85	1.0	This work

[1] CPE: Carbon Paste Electrode

[2] CMAB: cetyltrimethyl ammonium bromide

[3] GCE: Glassy Carbon Electrode

[4] PGH: Pyrolytic Graphite Electrode

[5] SPCE: Screen–Printed Carbon Electrode

*Detection limit

The stability and reproducibility of the sensor were also evaluated. Firstly, to investigate the stability of the sensors, five successive measurements of 10 nM T_4 were made at the same sensor, refreshed after each measurement by successive CV sweeps between −0.3 and +1.2 V vs. Ag/AgCl at scan rate of 50 mV·s^{-1}. After five successive amperometric experiments carried out under the same experimental conditions, the relative standard deviation (RSD) was 4.6 %. Secondly, three different β–CD-SH/Au–NPs@rGO/epoxy sensors were prepared and evaluated in order to compare their amperometric current responses. An aliquot of 10 nM T_4 was evaluated by triplicate with three different electrodes. The resulting RSD was 0.6 %, confirming that the preparation method was highly reproducible. Thirdly, multiple calibration experiments were also performed with these three nanocomposite sensors after polishing in order to estimate the reproducibility of the electrode surface. Contrary to most studies in which the (bio)recognition agents are attached on the electrode surface, in the presented work the recognition agent is dispersed the polymeric matrix and consequently is fixed in bulk. Experiments after five polishing processes demonstrated that the β–CD-SH/Au–NPs@rGO hybrid-nanomaterial was homogeneously well dispersed within the epoxy matrix, and no significant differences in sensitivity were observed (RSD of 3.8 %).

The sensors based on nanocomposites also present other benefits. Thanks to their easy surface regeneration by simple polishing between calibrations, a homogeneous distribution of the modifier agents in the nanocomposite would be obtained after each polishing. This fact guarantees that a reproducible electrode surface is obtained and the properties of the system are maintained.

In concordance with literature, it is also important to highlight that the influence of some typical electroactive biomolecules such as uric acid, ascorbic acid, dopamine, cholesterol and tyrosine do not present significant interferences on the current response of T_4 at carbon–based electrodes at the potential pertaining to the oxidation of thyroxine [11, 42]. In addition, although other biomarkers could be recognized by the β–CD-SH, it is expected that they would not interfere because the β–CD-SH agent is only used as a preconcentration agent on the electrode surface for the T_4 oxidation at +0.85 V vs. Ag/AgCl. Thus, the presented system clearly shows its potential for use in analysis in real samples, which will be studied in future.

Conclusions

We have synthesized a graphene–based hybrid-nanomaterial (the β–CD-SH/Au–NP@rGO) for the development of a sensitive T_4 amperometric sensor by the incorporation of β–CD-SH as a biorecognition agent onto the graphene–based electronic transducer via supramolecular chemistry, which might be also deposited onto screen-printed platforms for the fabrication of disposable electrodes.

Different rGO–based modified-sensors containing the recognition agent have been fabricated (β–CD-SH/rGO/epoxy and β–CD-SH/Au–NP@rGO/epoxy electrodes), demonstrating that the incorporation of Au–NPs was a key step in improving the electrical properties of the graphene. It is the first time, from our knowledge, that a graphene–based NPC sensor is used for sensing purposes.

The β–CD-SH/Au–NP@rGO/epoxy device presents the lowest detection limit regarding to those carbon–based electrochemical electrodes found in literature. Thus, the electrochemical properties of the NPC sensor combined together with its tunable sensitivity open up a wide range of applications in interesting clinical, pharmacological and biomedical investigations. Furthermore, the fact that the β–CD-SH was successfully integrated in the polymeric matrix allows for an

easy regeneration of the sensor surface by a simple polishing. This fact allows the biorecognition device to be comfortably integrated as a detector in an automated flow analyzer. These advancements will also allow for the development of a fast, inexpensive and transportable device for T_4 in situ detection, which might be applied in interesting clinical, pharmacological and biomedical investigations.

References

1. Epstein FH, Brent GA (1994) The molecular basis of thyroid hormone action. N Engl J Med 331(13):847–853
2. Hall JE (2010) Guyton and hall textbook of medical physiology. Elsevier Health Sciences, Philadelphia
3. Karapitta CD, Xenakis A, Papadimitriou A, Sotiroudis TG (2001) A new homogeneous enzyme immunoassay for thyroxine using glycogen phosphorylase b–thyroxine conjugates. Clin Chim Acta 308(1):99–106
4. Gök E, Ateş S (2004) Determination of thyroxine hormone by luminol chemiluminescence. Anal Chim Acta 505(1):125–127
5. Kahric-Janicic N, Soldin SJ, Soldin OP, West T, Gu J, Jonklaas J (2007) Tandem mass spectrometry improves the accuracy of free thyroxine measurements during pregnancy. Thyroid 17(4):303–311
6. Samanidou V, Gika H, Papadoyannis I (2000) Rapid HPLC analysis of thyroid gland hormones tri-iodothyronine (T3) and thyroxine (T4) in human biological fluids after SPE 23(5):681–692
7. Jacobsen E, Fonahn W (1980) Determination of 1-thyroxdine sodium and 1-triiodo- thyronine sodium in tablets by differential pulse polarography. Anal Chim Acta 119(1):33–38
8. Iwamoto M, Webber A, Osteryoung RA (1984) Cathodic reduction of thyroxine and related compounds on silver. Anal Chem 56(8):1202–1206
9. Wang F, Fei J, Hu S (2004) The influence of cetyltrimethyl ammonium bromide on electrochemical properties of thyroxine reduction at carbon nanotubes modified electrode. Colloids Surf B: Biointerfaces 39(1–2):95–101
10. He Q, Dang X, Hu C, Hu S (2004) The effect of cetyltrimethyl ammonium bromide on the electrochemical determination of thyroxine. Colloids Surf B: Biointerfaces 35(2):93–98
11. Wu K, Ji X, Fei J, Hu S (2004) The fabrication of a carbon nanotube film on a glassy carbon electrode and its application to determining thyroxine. Nanotechnology 15(3):287
12. Olivé-Monllau R, Pereira A, Bartrolí J, Baeza M, Céspedes F (2010) Highly sensitive CNT composite amperometric sensors integrated in an automated flow system for the determination of free chlorine in waters. Talanta 81(4):1593–1598
13. Muñoz J, Bartrolí J, Céspedes F, Baeza M (2015) Influence of raw carbon nanotubes diameter for the optimization of the load composition ratio in epoxy amperometric composite sensors. J Mater Sci 50(2):652–661
14. Muñoz J, Céspedes F, Baeza M (2015) Effect of carbon nanotubes purification on electroanalytical response of near-percolation amperometric nanocomposite sensors. J Electrochem Soc 162(8):B217–B224
15. Martín A, Batalla P, Hernández-Ferrer J, Martínez MT, Escarpa A (2015) Graphene oxide nanoribbon-based sensors for the simultaneous bio-electrochemical enantiomeric resolution and analysis of amino acid biomarkers. Biosens Bioelectron 68:163–167
16. Chen D, Tang L, Li J (2010) Graphene-based materials in electrochemistry. Chem Soc Rev 39(8):3157–3180
17. Martín A, Escarpa A (2014) Graphene: the cutting–edge interaction between chemistry and electrochemistry. TrAC Trends Anal Chem 56:13–26
18. Shin HJ, Kim KK, Benayad A, Yoon SM, Park HK, Jung IS, Jin MH, Jeong HK, Kim JM, Choi JY (2009) Efficient reduction of graphite oxide by sodium borohydride and its effect on electrical conductance. Adv Funct Mater 19(12):1987–1992
19. Fan Y, Liu J-H, Yang C-P, Yu M, Liu P (2011) Graphene–polyaniline composite film modified electrode for voltammetric determination of 4-aminophenol. Sensors Actuators B Chem 157(2):669–674
20. Compton OC, Nguyen ST (2010) Graphene oxide, highly reduced graphene oxide, and graphene: Versatile Building blocks for carbon-based materials. Small 6(6):711–723
21. Jasuja K, Berry V (2009) Implantation and growth of dendritic gold nanostructures on graphene derivatives: electrical property tailoring and Raman enhancement. ACS Nano 3(8):2358–2366
22. Fang Y, Guo S, Zhu C, Zhai Y, Wang E (2010) Self-assembly of cationic polyelectrolyte-functionalized graphene nanosheets and gold nanoparticles: A two-dimensional heterostructure for hydrogen peroxide sensing. Langmuir 26(13):11277–11282
23. Shahgaldian P, Pieles U (2006) Cyclodextrin derivatives as chiral supramolecular receptors for enantioselective sensing. Sensors 6(6):593–615
24. González-Campo A, Hsu S-H, Puig L, Huskens J, Reinhoudt DN, Velders AH (2010) Orthogonal covalent and noncovalent functionalization of cyclodextrin-alkyne patterned surfaces. J Am Chem Soc 132(33):11434–11436
25. Shahgaldian P, Hegner M, Pieles U (2005) A cyclodextrin self-assembled monolayer (SAM) based surface Plasmon resonance (SPR) sensor for enantioselective analysis of thyroxine. J Incl Phenom Macrocycl Chem 53(1–2):35–39
26. Rojas MT, Koeniger R, Stoddart JF, Kaifer AE (1995) Supported monolayers containing preformed binding sites. Synthesis and Interfacial Binding Properties of a Thiolated Beta-Cyclodextrin Derivative Journal of the American Chemical Society 117(1):336–343
27. Hummers WS Jr, Offeman RE (1958) Preparation of graphitic oxide. J Am Chem Soc 80(6):1339–1339
28. Fernandez-Merino M, Guardia L, Paredes J, Villar-Rodil S, Solis-Fernandez P, Martinez-Alonso A, Tascon J (2010) Vitamin C is an ideal substitute for hydrazine in the reduction of graphene oxide suspensions. J Phys Chem C 114(14):6426–6432
29. Tom RT, Suryanarayanan V, Reddy PG, Baskaran S, Pradeep T (2004) Ciprofloxacin-protected gold nanoparticles. Langmuir 20(5):1909–1914
30. Pumera M, Merkoçi A, Alegret S (2006) Carbon nanotube-epoxy composites for electrochemical sensing. Sensors Actuators B Chem 113(2):617–622
31. Chitravathi S, Kumara Swamy BE, Chandra U, Mamatha GP, Sherigara BS (2010) Electrocatalytic oxidation of sodium levothyroxine with phenyl hydrazine as a mediator at carbon paste electrode: A cyclic voltammetric study. J Electroanal Chem 645(1):10–15
32. Muñoz J, Céspedes F, Baeza M (2015) Modified multiwalled carbon nanotube/epoxy amperometric nanocomposite sensors with

CuO nanoparticles for electrocatalytic detection of free chlorine. Microchem J 122:189–196

33. Zhao H, Ji X, Wang B, Wang N, Li X, Ni R, Ren J (2015) An Ultrasensitive acetylcholinesterase biosensor based on reduced graphene oxide-Au nanoparticles-β-cyclodextrin/Prussian blue-chitosan nanocomposites for organophosphorus pesticides detection. Biosens Bioelectron 65:23–30

34. Zhang J, Yang H, Shen G, Cheng P, Zhang J, Guo S (2010) Reduction of graphene oxide via L-ascorbic acid. Chem Commun 46(7):1112–1114

35. Huang J, Zhang L, Chen B, Ji N, Chen F, Zhang Y, Zhang Z (2010) Nanocomposites of size-controlled gold nanoparticles and graphene oxide: formation and applications in SERS and catalysis. Nanoscale 2(12):2733–2738

36. Martin C, Sandler J, Shaffer M, Schwarz M-K, Bauhofer W, Schulte K, Windle A (2004) Formation of percolating networks in multi-wall carbon-nanotube–epoxy composites. Compos Sci Technol 64(15):2309–2316

37. Ramírez-García S, Alegret S, Céspedes F, Forster RJ (2004) Carbon composite microelectrodes: charge percolation and electroanalytical performance. Anal Chem 76(3):503–512

38. Rao CN, Sood AK, Subrahmanyam KS, Govindaraj A (2009) Graphene: the new two-dimensional nanomaterial. Angew Chem Int Ed 48 (42):7752–7777

39. Muñoz J, Bastos-Arrieta J, Muñoz M, Muraviev D, Céspedes F, Baeza M (2014) Simple green routes for the customized preparation of sensitive carbon nanotubes/epoxy nanocomposite electrodes with functional metal nanoparticles. RSC Advances 4(84):44517–44524

40. Raj MA, John SA (2015) Assembly of gold nanoparticles on graphene film via electroless deposition: spontaneous reduction of Au 3+ ions by graphene film. RSC Advances 5(7):4964–4971

41. Khafaji M, Shahrokhian S, Ghalkhani M (2011) Electrochemistry of levo-thyroxin on Edge-plane pyrolytic graphite electrode: application to sensitive analytical determinations. Electroanalysis 23(8):1875–1880

42. Das A, Sangaranarayanan M (2014) Electroanalytical sensor based on unmodified screen-printed carbon electrode for the determination of levo-thyroxine. Electroanalysis 27(2):360–367